ACS Chemical Neuroscience

Research Article

pubs.acs.org/chemneuro

Stochastic Formation of Fibrillar and Amorphous Superoxide Dismutase Oligomers Linked to Amyotrophic Lateral Sclerosis

Alireza Abdolvahabi,[†] Yunhua Shi,[†] Aleksandra Chuprin,[†] Sanaz Rasouli,[†,‡] and Bryan F. Shaw*[,†]

[†]Department of Chemistry and Biochemistry, and [‡]Institute of Biomedical Studies, Baylor University, Waco, Texas 76798-7348, United States

Supporting Information

ABSTRACT: Recent reports suggest that the nucleation and propagation of oligomeric superoxide dismutase-1 (SOD1) is effectively stochastic in vivo and in vitro. This perplexing kinetic variability—observed for other proteins and frequently attributed to experimental error—plagues attempts to discern how *SOD1* mutations and post-translational modifications linked to amyotrophic lateral sclerosis (ALS) affect SOD1 aggregation. This study used microplate fluorescence spectroscopy and dynamic light scattering to measure rates of fibrillar and amorphous SOD1 aggregation at high iteration ($n_{total} = 1.2 \times 10^3$). Rates of oligomerization were intrinsically irreproducible and populated continuous probability distributions. Modifying reaction conditions to mimic random and systematic experimental error could not account for kinetic outliers in standard assays, suggesting that stochasticity is not an experimental artifact, rather an intrinsic property of SOD1 oligomerization (presumably caused by competing pathways of oligomerization). Moreover, mean rates of fibrillar and amorphous nucleation were not uniformly increased by mutations that cause ALS; however, mutations did increase kinetic noise (variation) associated with nucleation and propagation. The stochastic aggregation of SOD1 provides a plausible statistical framework to rationalize how a pathogenic mutation can increase the probability of oligomer nucleation within a single cell, without increasing the mean rate of nucleation across an entire population of cells.

KEYWORDS: *Copper, zinc, protein aggregation, amyloid, oligomerization, amyotrophic lateral sclerosis*

The prionlike aggregation of wild-type (WT) and mutant superoxide dismutase-1 (SOD1) in neuronal cells, followed by propagation to neighboring neurons, is linked to a fraction of familial and sporadic amyotrophic lateral sclerosis (ALS) cases.[1−6] It remains unclear whether *SOD1* mutations induce cytotoxicity by accelerating the intrinsic rate of SOD1 oligomerization, or by a separate mechanism, for example, by increasing the cytotoxicity of an SOD1 oligomer, irrespective of its rate of formation. This question remains unanswered, in part, because it remains unknown whether the stochastic aggregation of SOD1, observed in vitro and in vivo,[7,8] is a thermodynamic property of SOD1 self-assembly, or an experimental artifact generated by random or systematic error. This lack of clarity has made it technically challenging to precisely quantify how ALS-linked mutations in *SOD1* affect the actual rate (or mean rate) of nucleation and propagation of oligomeric SOD1.

Statistical analysis of amyloid nucleation and elongation rates for several proteins suggests that amyloidogenesis is intrinsically stochastic;[7,9,10] that is, measured rates span a continuous probability distribution that cannot be explained by experimental error.[11−15] Other studies invoke deterministic models,[16] but report replicate rates that span a distribution of inexplicable breadth.[16] Models of stochastic nucleation are generally invoked to explain the irreproducible rates of self-assembly of systems across all size scales, from the crystallization of H_2O[11] and the aggregation of proteins[10] and mRNA,[17] to gene expression[18] and the mesoscale aggregation of social amoeba.[19] The intrinsic irreproducibility associated with measuring rates of these processes can be circumvented by collecting high numbers of replicate measurements (on the order of $n = 10^2$) and calculating statistically significant rates and population comparisons.[11] In the case of amyloid self-assembly, the reproducibility of kinetic assays can be increased by the addition of "seed" oligomers,[10,20] but this type of seeding presumably bypasses the stochastic steps of primary nucleation.

Received: February 17, 2016
Accepted: March 15, 2016
Published: March 15, 2016

DOI: 10.1021/acschemneuro.6b00048
ACS Chem. Neurosci. 2016, 7, 799−810

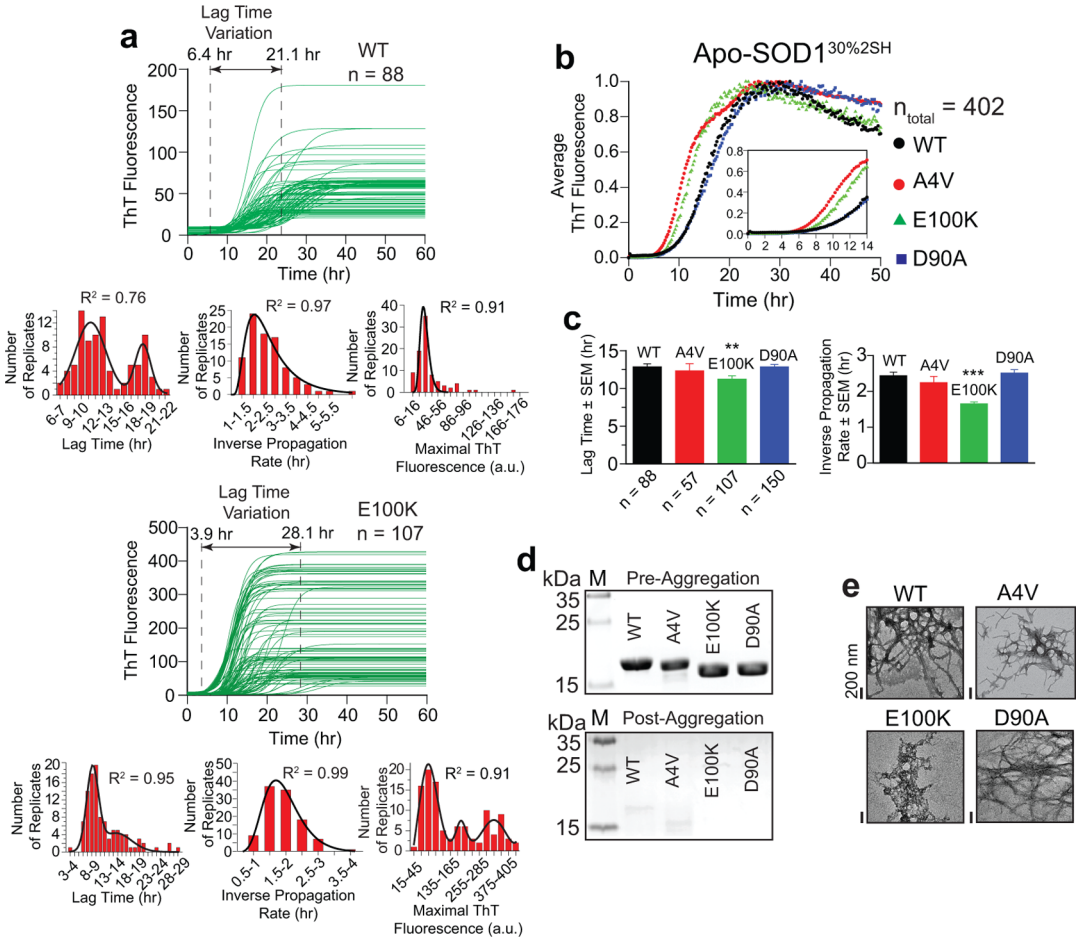

Figure 1. In vitro fibrillization of apo-SOD1 in microplate-based ThT fluorescence assays. (a) Sigmoidal fits of ThT fluorescence of replicate assays of WT and E100K apo-SOD1$^{30\%2SH}$ carried out in 96-well microplates with mechanical agitation (37 °C, pH 7.4, 150 mM NaCl, 10 mM TCEP, i.e., apo-SOD1$^{30\%2SH}$). Histograms of iterate lag time, inverse propagation rate, and maximal ThT fluorescence are shown as insets below each plot, fit with either a 3-parameter log−normal distribution (eq S2a) or a Lorentzian bimodal function (eq S3). (b) Average and normalized plots of replicate ThT amyloid assays from (a). (c) Mean lag time and inverse propagation rate for all apo-SOD1$^{30\%2SH}$ proteins ($p < 0.0001$***; $p < 0.01$**). (d) Upper gel: SDS-PAGE of WT and ALS-variant apo-SOD1$^{30\%2SH}$ solutions performed before ThT assay. Lower gel: SDS-PAGE of supernatant of same solutions after ThT aggregation assay and centrifugation. (e) TEM analysis of apo-SOD1$^{30\%2SH}$ fibril homogenates after the completion of aggregation assay.

Two of our previous investigations into the fibrillization of apo-SOD1 uncovered a high degree of irreproducibility, when using thioflavin-T fluorescence assays to measure "unseeded" amyloid fibril nucleation and propagation.[21,22] For example, the lag time of WT apo-SOD1 fibrillization varied by up to 68% and propagation rates by up to 50% in *replicate* measurements that were made simultaneously in a 96-well plate, on sample aliquots from the same, filtered stock solution of pure apo-SOD1.[21,22] Other investigations into apo-SOD1 oligomerization have not reported this apparent stochasticity,[1,23−25] with the exception of a recent report by Lang and co-workers.[7] Although these previous studies suggest that the fibrillization of apo-SOD1 is stochastic, there have been no investigations into whether sample-to-sample variations in reaction conditions and/or competing pathways of non-fibrillar aggregation are a source of this apparent stochasticity. Resolving why SOD1 aggregation is apparently stochastic during in vitro assays is relevant to understanding its aggregation in vivo. For example, the aggregation of ALS mutant SOD1 in transgenic mouse models of ALS appears to follow the same sigmoidal, stochastic nucleation kinetics observed in vitro with the types of assays used in the current study (microplate-based, thioflavin-T fluorescence assays that employ mechanical agitation).[7,26−29]

RESULTS AND DISCUSSION

Apo-SOD1 Fibrillization Is Effectively Stochastic. Thioflavin-T (ThT) fluorescence was used to measure the "unseeded" rate of nucleation and propagation of amyloid fibrils for WT and three biophysically diverse ALS-variant apo-SOD1 proteins, including A4V (which is intrinsically disordered in the disulfide-reduced apo state) and two "cryptic" variants, D90A and E100K (which have subtle effects on the structure and conformational stability of apo-SOD1).[30] Microplate assays utilized mechanical agitation (i.e., a gyrating Teflon bead) to accelerate aggregation (possibly inducing fragmentation of elongating fibrils[31]). A total of 1132 ThT assays were made for all four proteins at a variety of experimental conditions.

Rates of aggregation were measured at two degrees of disulfide reduction, that is, 30% reduced (denoted as apo-SOD1$^{30\%2SH}$, Figure 1) and ∼90% reduced (denoted as apo-SOD1$^{90\%2SH}$, Figure 2) achieved by incubating apo-SOD1 in 10 mM or 100 mM TCEP, respectively, for 6 h prior to assay. The semireduced state (i.e., apo-SOD1$^{30\%2SH}$) was chosen to mimic the gradual reduction of apo-SOD1 proteins that will occur intracellularly upon loss of metal ions,[32] whereas the more fully reduced state (i.e., apo-SOD1$^{90\%2SH}$) was utilized to mimic the self-assembly of

DOI: 10.1021/acschemneuro.6b00048
ACS Chem. Neurosci. 2016, 7, 799−810

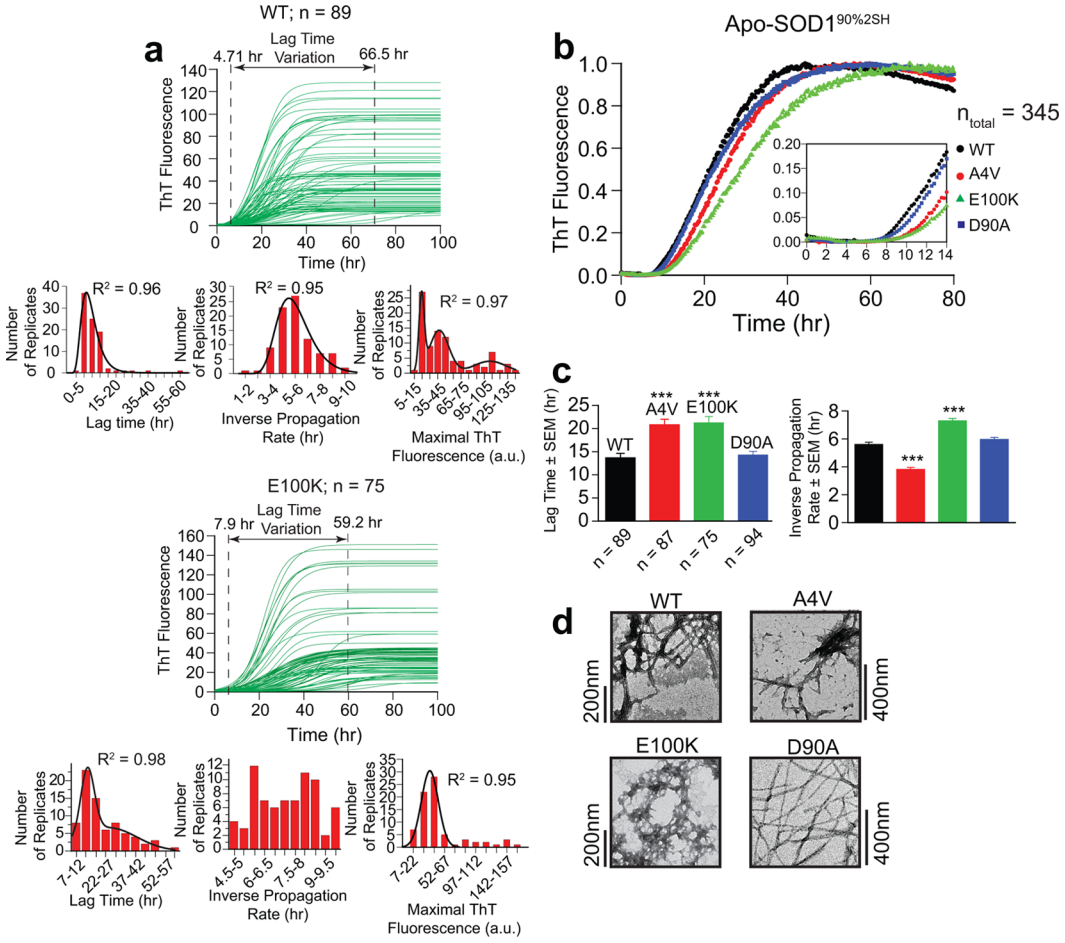

Figure 2. Increasing the degree of disulfide reduction from 30% to 90% does not eliminate the stochasticity of apo-SOD1 fibrillization in microplate-based ThT fluorescence assays. (a) Sigmoidal fits of ThT fluorescence of replicate assays of WT and E100K apo-SOD1$^{90\%2SH}$. Histograms of lag time, inverse propagation rate, and maximal ThT fluorescence are shown as insets below each plot and are fit with either a 3-parameter log-normal distribution (eq S2a) or bimodal Lorentzian function (eq S3). (b) Average and normalized plots of ThT fluorescence for all apo-SOD1$^{90\%2SH}$ proteins. (c) Mean lag time and inverse propagation rate for apo-SOD1$^{90\%2SH}$ ($p < 0.0001$***). (d) TEM micrographs of apo-SOD1$^{90\%2SH}$ at the end of aggregation assay.

nascent protein immediately after translation.[1] The degree of disulfide reduction was determined with differential scanning calorimetry (DSC) and size-exclusion chromatography (SE-HPLC), per the effect of disulfide reduction on the monomerization of apo-SOD1 and lowering of its melting transition temperature (Figure S1).[33,34] Analysis of each apo-SOD1 protein with ICP-MS, DSC, and SE-HPLC confirmed that each set of proteins was demetalated (<0.04 Zn^{2+} and <0.02 Cu^{2+} per monomer, Table S1), properly folded (or disordered in the case of disulfide reduced A4V), and pure before each ThT assay (Figure S1 and Table S1). In this study, we only examined the aggregation rates of metal free SOD1, without the influence of metal ions on aggregation. Although the removal of metal ions typically increases the rate of SOD1 aggregation, recent studies have shown that the aberrant binding of zinc to SOD1 can trigger amorphous aggregation.[35]

A variation in lag time of more than 15 h, and a variation in inverse propagation rate constant of several hours, was observed among replicate measurements for all ThT assays of apo-SOD1$^{30\%2SH}$ proteins at 37 °C, pH 7.4 (Figures 1a and S2). This kinetic variability occurred even though replicate measurements were performed on aliquots from the same, filtered stock solution, and analyzed simultaneously in 96-well plates. This magnitude of kinetic variation has been observed in the fibrillization of several other proteins including β_2 microglobulin, $A\beta_{(1-42)}$ amyloid peptide, sickle hemoglobin, and insulin.[9,10,13,14,36,37] Nonclassical stochastic nucleation models best describe the variations in nucleation and elongation of SOD1 amyloid fibrils.[12,38−40] Discarding any kinetic outliers based upon statistical tests (e.g., Dixon's Q test) is inappropriate because there is no reason to suspect, ab initio, that outliers were caused by error[22] (this point is investigated in detail below). Evaporation from sealed wells, for example, cannot account for these variations: measurement of volume of wells exhibiting outlier aggregation kinetics (with a micropipette at the end of each assay) revealed that volumes varied by < ±3.5% from the mean volume of wells. We hypothesize that variations in the rate of nucleation are caused by (i) variations in the activation energy (E_a) of amyloid nuclei that formed in different wells, and/or (ii) off-amyloid pathways of aggregation that compete with amyloid formation and diminish the concentration of unassembled SOD1, for example, formation of amorphous aggregates.[41] For example, the early formation of amorphous aggregates (possibly also stochastic) would not be detected in the ThT assay, but would lower the concentration of free apo-SOD1 available to fibrillize which could explain ThT plots that exhibited increased lag time of fibrillization, decreased elongation rates, and decreased maximal ThT fluorescence (Figures 1a and S2).

Histograms of fibril propagation (expressed as $1/k$) generally exhibited a log-normal behavior (eqs S2a and b), where lag time

DOI: 10.1021/acschemneuro.6b00048
ACS Chem. Neurosci. 2016, 7, 799−810

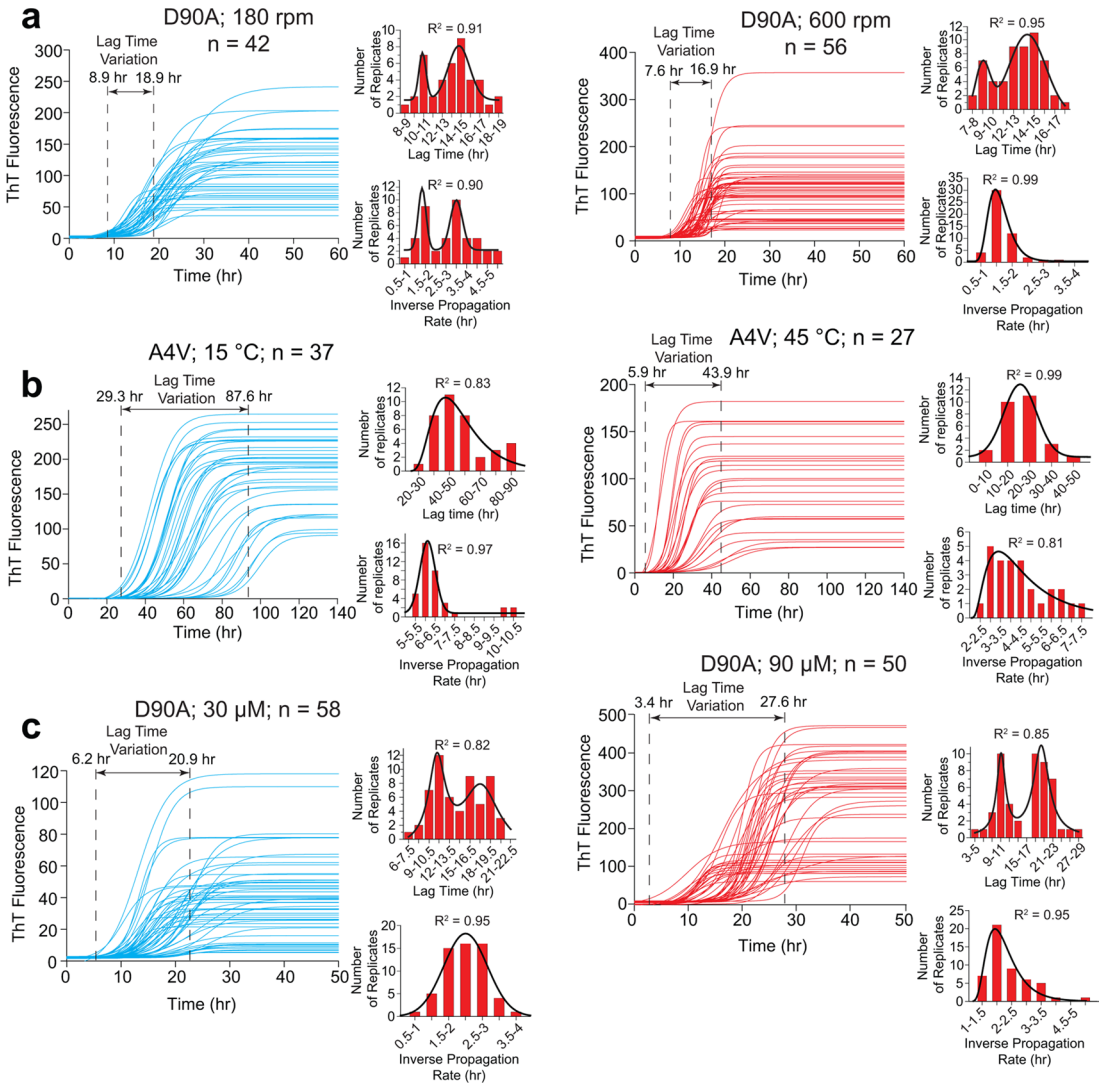

Figure 3. Alteration of experimental conditions (SOD1 concentration, gyration rate, and temperature) to mimic possible well-to-well variations in reaction conditions during microplate-based ThT assays of apo-SOD1 fibrillization. (a) ThT fluorescence assays of D90A apo-SOD1$^{30\%2SH}$ at different gyration speeds. (b) ThT fluorescence assays of A4V apo-SOD1$^{90\%2SH}$ at 15 and 45 °C. (c) ThT fluorescence assays at varying [D90A apo-SOD1$^{30\%2SH}$]. Insets next to each plot represent the histograms of lag time and inverse propagation rate. Histograms were fit with either a 4-parameter log-normal function (eq S2b) or a bimodal Lorentzian distribution function (eq S3), except for the histograms of lag time at 45 °C and propagation rate at 30 μM that showed normal distributions.

generally exhibited a bimodal Lorentzian distribution (eq S3) with $R^2_{average} > 0.7$. Measuring apo-SOD1 fibrillization at such high iteration allowed us to conclude—with statistical significance—that ALS mutations do not uniformly decrease the mean lag time of apo-SOD1 fibrillization, at least at 30% reduction (Figure 1b,c and Table S2). In fact, the A4V and D90A substitutions in apo-SOD1$^{30\%2SH}$ have statistically similar lag times of fibrillization as WT protein ($p > 0.05$). Moreover, A4V and D90A mutations did not uniformly accelerate the propagation (elongation rate) of apo-SOD1$^{30\%2SH}$ fibrillization under semireduced conditions (Figure 1b,c and Table S2).

The observed variation in lag time, propagation, and maximal ThT fluorescence was not caused by the presence of residual monomeric/dimeric SOD1 in each well (i.e., a lack of complete aggregation). For example, SDS-PAGE of protein supernatant at the end of the ThT assay confirmed that apo-SOD1 proteins were incorporated into a sedimentable aggregate, with no residual monomer (Figure 1d). The morphology of apo-SOD1 aggregates generated during ThT assays was characterized with transmission electron microscopy (TEM), and found to be, generally, a mixture of fibrillar and amorphous species (Figure 1e).

Increasing the degree of disulfide reduction, from 30% to 90% did not improve the reproducibility of amyloid assays (Figures 2a and S3). We point out that ALS mutations do not uniformly accelerate the nucleation and propagation (Figure 2b,c and Table S2) and morphology (Figure 2d) of apo-SOD1, even at 90% reduction. This result is contrary to previous reports, that ALS mutations uniformly accelerate apo-SOD1 aggregation.[7,24,25]

Well-to-Well Variation in Reaction Conditions Cannot Explain Observed Stochasticity of Apo-SOD1 Fibrillization. We sought to determine if the observed stochasticity of SOD1 fibrillization, in particular, the presence of slowly aggregating wells, was an experimental artifact that was caused by well-to-well variations in (i) the orbital velocity of each Teflon bead, (ii) the local temperature of each well (due to nonuniform heating or friction of the gyrating polystyrene microplate), (iii) variations in the mass or surface properties of one stirring bead,

DOI: 10.1021/acschemneuro.6b00048
ACS Chem. Neurosci. 2016, 7, 799−810

compared to the next, (iv) surface features (i.e., scratches) of one well compared to next, or (v) the presence of contaminants such as common dust particles. For example, we concede that it is possible that wells exhibiting outlier kinetics ("outlier wells") in Figure 1, which aggregated with late lag times, were slow to fibrillize because Teflon beads were failing (for some reason) to orbit circularly in the well at the same mean velocity (rpm) as beads in other wells. To test this hypothesis, we performed ThT assays on D90A apo-SOD1$^{30\%2SH}$ at 180 and 600 rpm. We found that changing gyration speed by 3-fold did not alter mean lag time by a magnitude sufficient to account for outlier lag times at 360 rpm (Figure 3a). In fact, a linear correlation between lag time and shaking speed was found to be only 0.0041 h/rpm (Figure S4), which is insufficient to explain 15 to 30 h variation in lag time among wells. The correlation in rpm and lag time translates to a correlation of shear force and gyration speed of 0.13 nN/rpm.

Varying the temperature of the microplate from 15 to 45 °C, that is, by a magnitude much larger than any expected well-to-well thermal variation in the temperature controlled fluorescence plate reader, slightly affected the variation in the lag time of fibrillization of A4V apo-SOD1 (Figure 3b). However, this temperature alteration (15−45 °C) resulted in $\Delta\tau_{mean}$ = 1.01 h/30 °C, which is insufficient to account for >15 h variation in lag times observed at 37 °C (Figure S5). We chose to perform the temperature-specific experiments on A4V apo-SOD1$^{90\%SH}$ because this ALS-variant protein is intrinsically disordered and changes in temperature from 15 to 45 °C will not affect its degree of folding as much as ordered proteins.[42] Varying SOD1 concentrations revealed that the mean lag time of D90A apo-SOD1$^{30\%2SH}$ fibrillization increased with apo-SOD1 concentration by only 0.2 h·μM^{-1}, which is insufficient to explain the >15 h variation in lag time that we observed in replicate experiments of apo-SOD1 (the D90A apo-SOD1 protein was used for these experiments, per availability) (Figure 3c).

The effect of gyration speed (rpm), protein concentration, and temperature on the average noise (η) of each assay can be found in the Supporting Information (Figure S6). By "noise", we refer to the coefficient of variation, that is calculated at each time point as $\eta = \sigma/I_{avg}$, where I_{avg} is the mean intensity of fluorescence of all replicate measurements at a given time point and σ is the standard deviation of mean intensity.

It is possible that some surface features of a specific well or bead (e.g., a scratch or lack thereof, or slight difference between the mass of different Teflon beads) could be the cause of outlier kinetics and apparent stochasticity. To test this hypothesis, we repeated aggregation assays in specific wells, and reused the same Teflon bead (Figure 4a). For these experiments, a specific well and bead that resulted in outlier kinetics were washed with near-boiling SDS, followed by guanidinium hydrochloride, followed by incubation and washing with pepsin solutions to remove any adhered residual aggregates. Aggregation assays were then repeated in these identical wells (using the identical Teflon bead) under the exact same conditions, using apo-SOD1 proteins from the same "mother" stock. The initial rate of aggregation could not be uniformly replicated by repeating assays in the same microplate well, with the same bead (see dashed and solid traces, Figure 4a). We point out that small variations in the mass of different Teflon beads likely do not account for stochasticity observed in Figure 1a. The 3.18 mm diameter Teflon beads were found to vary in mass by only ±0.35 mg (from 36.20 to 36.90 mg).

Anecdotal evidence suggests that the intrinsic irreproducibility of many amyloid assays is caused by the nonuniform presence of

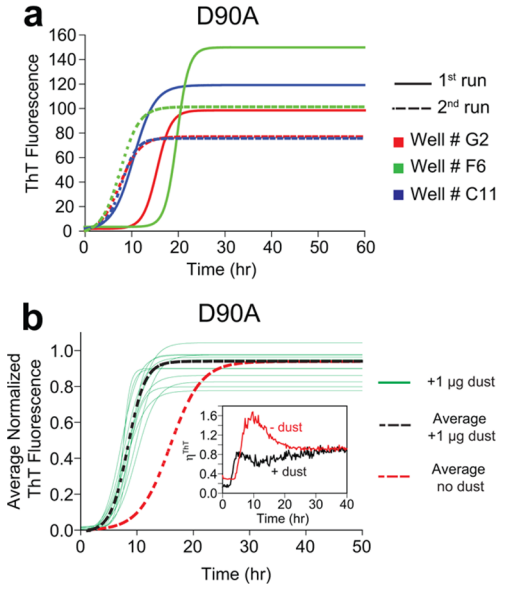

Figure 4. Stochastic fibrillization of apo-SOD1 in microplate ThT assays is not an artifact of surface features in a microplate well (or bead), and is not caused by dust contamination from laboratory environment. (a) Repetition of ThT assays in identical microplate wells (washed and reused), with identical Teflon beads (washed and reused) does not abolish kinetic variability. (b) Fibrillization of D90A apo-SOD1$^{30\%2SH}$ in the presence of ~1 μg of dust particles collected from our laboratory windowsills (green traces and black dashed line, n = 12) and absence of dust particles (red dashed line), pH 7.4, 37 °C. Inset shows the plots of noise (η) associated with D90A apo-SOD1$^{30\%2SH}$ fibrillization in the presence and absence of room dust.

common dust particles that are inadvertently introduced in sample wells during laboratory preparation. Dust could conceivably accelerate aggregation via surface catalysis,[43,44] or decelerate aggregation (in the case of apo-SOD1) via Zn^{2+} contamination. Even though we filtered all solutions immediately before dispensing into each microplate, we tested this hypothesis (previously untested, to our knowledge) by deliberately contaminating wells with dust particles collected from bookshelves and windowsills of the Shaw laboratory (where all experiments were performed). Approximately 1 μg of lab dust—presumably more than could ever be expected to contaminate a single well—was added to wells, and ThT assays were performed on D90A apo-SOD1$^{30\%2SH}$. Dust particles decreased the mean lag time of fibrillization by 7.2 ± 0.3 h (Figure 4b), and decreased the inverse propagation rate constant from 2.52 ± 0.1 h to 1.51 ± 0.1 h. Moreover, dust contamination actually diminished the noise associated with lag time (inset in Figure 4b), as expected with a shorter lag time. Dust contamination cannot, therefore, account for the positive skewness of the probability distributions observed in Figure 1, that is, slow, outlier kinetics with lag times of 30−60 h.

We found a global correlation between the lag time and propagation rate of amyloid fibrillization for all four apo-SOD1 proteins analyzed in this study, under all reaction conditions, that is, temperature, gyration rate, protein concentration, reductant concentration (Figure 5; black circles). This correlation—observed for other proteins,[31,45] including apo-SOD1[7]—suggests that the product of lag time and propagation rate of apo-SOD1 fibrillization (α) is a constant value ($\alpha = \tau k$ = 2.5 ± 0.2), regardless of variations in experimental conditions (Figure 5). This value of α for SOD1 is smaller than α reported for other

DOI: 10.1021/acschemneuro.6b00048
ACS Chem. Neurosci. 2016, 7, 799−810

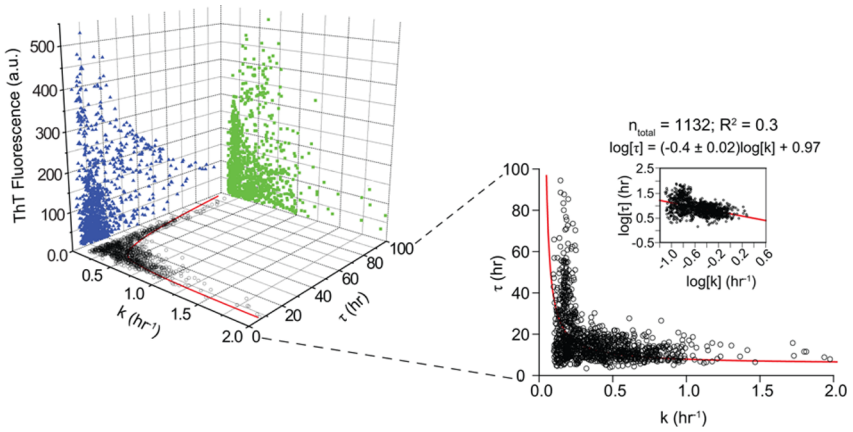

Figure 5. Projection plot of maximal ThT fluorescence, lag time, and propagation rate constant of apo-SOD1 fibrillization derived from all 1132 ThT assays of WT and mutant proteins collected under all reaction conditions in this study. Inset shows the projection of lag time versus elongation rate (black circles). Solid red trace is characterized by an α value ($\alpha = \tau k$) of 2.5 ± 0.2, and inset shows similar data in logarithmic scale.

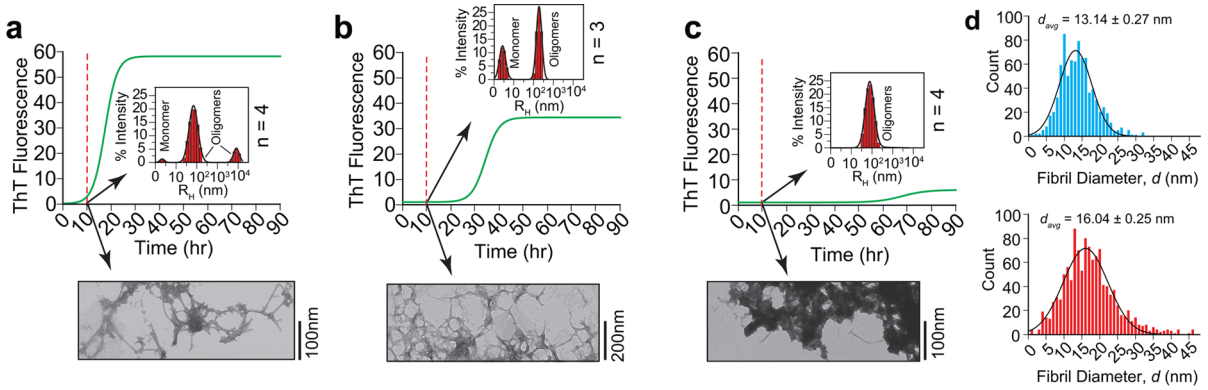

Figure 6. Comparison of oligomer morphology from replicate wells containing identical solutions of apo-SOD1. Plots of ThT fluorescence of A4V apo-SOD1$^{90\%2SH}$ are shown for (a) fast, (b) intermediate, and (c) slow outliers. Center insets show corresponding mean DLS regularization graphs at 10 h; n = number of replicate DLS measurements on wells with similar lag times (±2 h); monomeric apo-SOD1 has a radius of 1.9 nm.[46] Insets below each plot are TEM micrographs of wells at 10 h. (d) Fibril diameter measurements (from TEM micrographs) at the end of 168 h assay. Upper histogram shows the measurements for fast outlier in panel (a), and lower histogram shows the measurements for slow outlier in panel (c).

amyloidogenic polypeptides, for example, α = 4.5 for insulin, glucagon, and various toxic mutants of Aβ_{1-40},[45] but seems to suggest that the fibrillization mechanism of apo-SOD1 is similar to these proteins.[45] The maximal ThT fluorescence intensity also generally decreased with increasing lag time or rate (Figure 5; blue triangles and green squares); however, this correlation was not as strong as the logarithmic correlation between τ and k. The projection plots of ThT fluorescence do reveal boundary regions of allowable ThT fluorescence per lag time and propagation rate of a fibril, and vice versa.

Competition between Amorphous and Fibrillar Aggregation Pathways Explains Variability of ThT Assays. Dynamic light scattering and TEM were used to determine if wells that were slow to fibrillize during ThT assays contained monomeric SOD1 throughout the prelag phase (Figure 6). We do not suspect that such outlier wells were slow to fibrillize because they contained monomeric SOD1 that failed (for some reason) to aggregate, but rather because these wells rapidly formed a significant amount of amorphous aggregates before fibril nucleation, which lowered the concentration of free apo-SOD1 available to fibrillize. This mechanism would account for the trends of increased fibril lag time, decreased fibril propagation rate, and diminished maximal ThT fluorescence observed for outlier wells in Figures 1 and 2, and summarized in Figure 5.

To test this hypothesis, we briefly halted the ThT assays of A4V apo-SOD1$^{90\%2SH}$ aggregation after 10 h, that is, at a time point near the mean lag time, where several wells will and will not exhibit ThT fluorescence. Aliquots were quickly removed from 12 wells and the ThT assay was continued (each of these 12 wells eventually exhibited a sigmoidal increase in ThT fluorescence, of varying magnitude, with lag times between 12.8 and 58.3 h, Figure 6a–c). The 10 h aliquots were immediately examined with DLS and TEM (Figure 6a–c). DLS showed the presence of an oligomer in all 12 wells of R_H = 80 nm (R_H: hydrodynamic radius). This oligomer was even present in wells that went on to fibrillize with a ~60 h lag time, but exhibited zero baseline fluorescence at 10 h (Figure 6c). Only wells that exhibited early lag times in ThT assays contained larger assemblies (R_H = 8000 nm) that are presumably fibrillar SOD1 (Figure 6a). Wells that exhibited zero fluorescence at 10 h and lag times of ~60 h did not contain (at 10 h) monomeric SOD1 or oligomeric species with R_H = 8000 nm, but again contained only ThT-negative assemblies with R_H = 80 nm (Figure 6c). TEM revealed predominantly amorphous species in these wells with zero fluorescence at 10 h, and lag times of ~60 h. (Figure 6c). This result suggests that (i) wells with late lag time do not contain monomeric SOD1 during the entire prelag phase, (ii) amyloidogenesis is in competition, in the microplate assay, with

DOI: 10.1021/acschemneuro.6b00048
ACS Chem. Neurosci. 2016, 7, 799–810

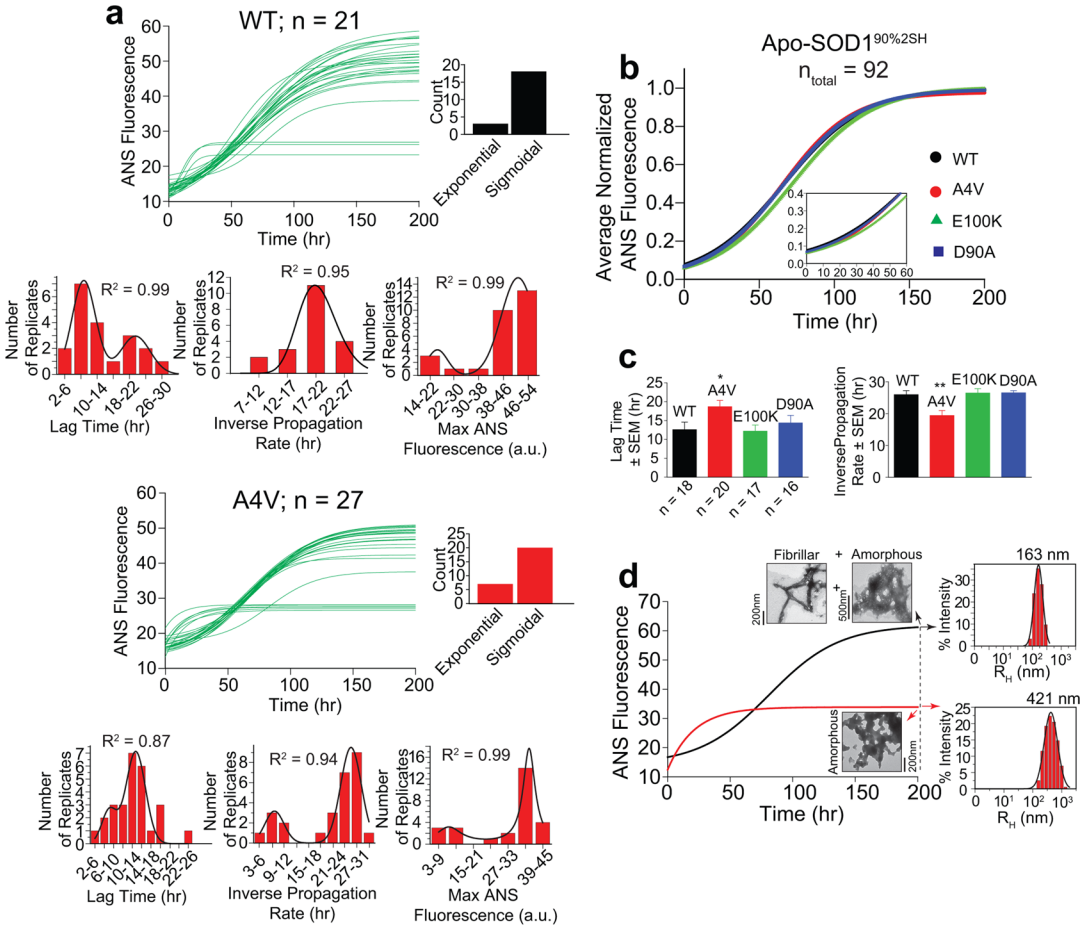

Figure 7. Distinct populations (microplate wells) of SOD1 stochastically diverge between exponential amorphous aggregation and sigmoidal amorphous/fibrillar aggregation according to DLS, TEM, and ANS fluorescence. (a) Plots of ANS fluorescence for WT and A4V apo-SOD1$^{90\%2SH}$ proteins (n_{total} = 48). Insets below each plot illustrate the histograms for lag time and inverse propagation rate. Inset next to each plot shows the comparison between the number of exponential and sigmoidal traces. (b) Average and normalized plots of ANS fluorescence for all apo-SOD1$^{90\%2SH}$ proteins (all data points included). Inset shows a magnification of lag phase. (c) Comparison plots of lag time and inverse propagation rate for all apo-SOD1$^{90\%2SH}$ proteins (*p < 0.05; **p < 0.01). (d) TEM micrographs and DLS regularization graphs of wells exhibiting exponential aggregating (red trace) and sigmoidal aggregating (black trace) at the end of the ANS fluorescence assay, that is, ∼200 h (traces are for E100K apo-SOD1$^{90\%2SH}$).

amorphous aggregation, and (iii) cooperativity between amorphous and fibrillar aggregation can explain (at least in part) why some wells form fibril nuclei early, propagate fibrils quickly, and exhibit high ThT fluorescence (Figure 6a), and why some wells fibrillize late, propagate slowly, and exhibit low ThT fluorescence, that is, these wells form, instead, early amorphous aggregates during the ThT assay (Figure 6c).

Although the TEM analysis of wells that exhibited slow or fast aggregation showed differences in the abundance of fibrillar versus amorphous aggregates (Figure 6a,c), we note that the fibrils that were present in both types of wells generally had similar fibril diameter (Figure 6d). The average diameter of fibrils in wells that exhibited fibrillization lag times of ∼10 h was 13.14 ± 0.27 nm, whereas wells with lag time of ∼60 h contained fibrils with average diameter of 16.04 ± 0.25 nm (Figure 6d).

To measure the kinetics of amorphous aggregation and further confirm that amorphous aggregation occurs quickly in certain wells, and more slowly in others, we performed ANS fluorescence assays on all fully reduced apo-SOD1 proteins (apo-SOD1$^{90\%2SH}$). Previous studies have utilized ANS to detect and study the formation kinetics of amorphous protein aggregates both in vitro and in vivo.[41,47] ANS has been shown to specifically bind to amorphous aggregates, however, ANS has also been reported to bind to amyloid fibrils but fluoresces reportedly more weakly than ThT.[47] Thus, ANS fluorescence is a suitable probe for detecting total aggregate formation.

The most striking result of ANS assays was that the aggregation of SOD1 in individual wells exhibited divergent, two-state behavior (Figures 7a,d and S7). For example, a minor fraction of wells (∼22%) exhibited exponential (fast) aggregation kinetics without a nucleation (lag) phase and with low maximal ANS fluorescence, whereas the majority of wells exhibited sigmoidal (slow) aggregation kinetics (Figures 7a,d and S7). Wells that underwent exponential aggregation plots showed weaker ANS fluorescence than sigmoidal ones, and larger aggregates (R_H ≈ 420 nm in exponential versus R_H ≈ 160 nm in sigmoidal, Figure 7d). We suspect that the weaker fluorescence in exponential wells compared to sigmoidal is due to light scattering, that is, ∼800 nm wide nonfibrillar particles will scatter or reflect 444 and 485 nm light more than fibrillar particles with hydrodynamic diameters of ∼320 nm. We analyzed these divergent wells with TEM to discern their morphology: wells with exponential kinetics contained amorphous aggregates without any traces of fibrillar structures (Figure 7d, red trace). Wells with sigmoidal kinetics contained both amorphous and fibrillar species (Figure 7d; black trace). This result suggests that

DOI: 10.1021/acschemneuro.6b00048
ACS Chem. Neurosci. 2016, 7, 799−810

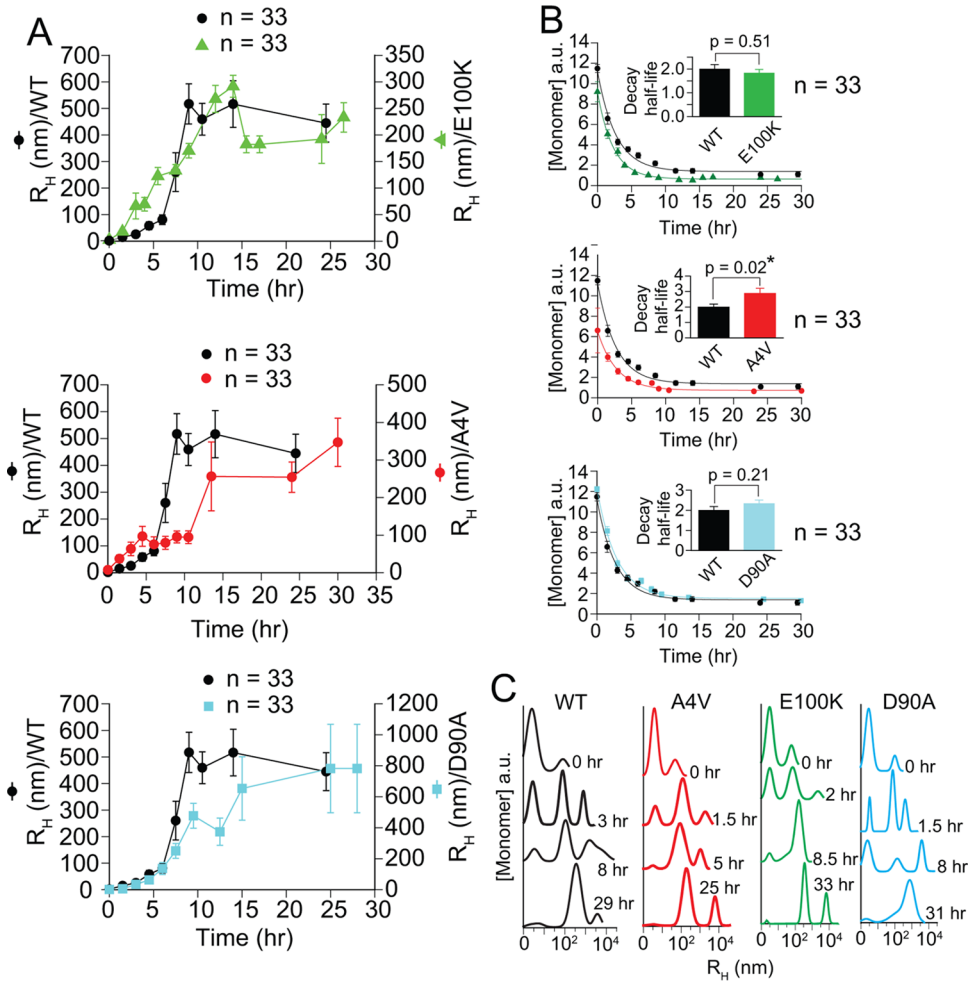

Figure 8. Formation of small oligomers and amorphous species of apo-SOD1 is nonuniformly accelerated by ALS mutations. (a) Dynamic light scattering (DLS) plots of aggregation of WT, E100K, A4V, and D90A apo-SOD1$^{90\%2SH}$. Average R_H expresses the average hydrodynamic radius of all species in sample (including any monomeric SOD1), expressed as mean ± SEM (n = 33). (b) SOD1 monomer decay plots of ALS-variant and WT apo-SOD1$^{90\%2SH}$ (derived from experiments in (a)). These plots were generated by the disappearance of monomeric SOD1 that appears at 1.9 nm. Insets show comparison of decay half-life for each protein (*p < 0.05), obtained by an exponential decay fit. (c) Representative DLS regularization graphs for all apo-SOD1$^{90\%2SH}$ proteins at different time points show the decay of monomer and formation of oligomers (from which plots in (b) are derived). Error bars express average ± SEM (n = 33).

discrete populations (wells) of SOD1 diverge stochastically between amorphous and fibrillar pathways. We hypothesize that isolated populations of SOD1 that exist in vivo , for example, a population isolated by virtue of being in a particular cell, can undergo similar stochastic divergence along different pathways of aggregation.

The sigmoidal aggregation of apo-SOD1 as measured by ANS fluorescence was generally more reproducible than sigmoidal fibrillization measured by ThT (Figures 2 and 7). For each protein, the lag times associated with sigmoidal ANS-positive aggregation of apo-SOD1$^{90\%2SH}$ proteins were within error of the lag times associated with ThT-positive aggregation (Tables S2 and S3), with the exception of E100K apo-SOD1$^{90\%2SH}$ which exhibited the highest number of wells with exponential aggregation (Figure S7a). The propagation rate of sigmoidal aggregation was, however, markedly slower (by up to 20 h) when measured by ANS fluorescence, compared to ThT (Figures 2b,c and 7b,c), an effect that might be caused by the inhibitory effect of ANS on protein aggregation, compared to ThT.[48]

We point out that none of the ALS mutations that we studied accelerated ANS-positive aggregate nucleation, compared to the WT protein (in the sigmoidal regime, Figure 7b,c). In fact, the A4V apo-SOD1$^{90\%2SH}$ protein exhibited a longer lag time (by 6.1 ± 2.6 h) compared to WT apo-SOD1$^{90\%2SH}$ in ANS assays (Figure 7b,c and Table S3). Moreover, ALS mutations did not uniformly accelerate propagation in ANS assays, for example, E100K and D90A apo-SOD1$^{90\%2SH}$ aggregated with propagation rates within the error of WT SOD1. The A4V mutation decreased the inverse rate of propagation of apo-SOD1$^{90\%2SH}$ by 6.5 ± 2.2 h (Figure 7b,c and Table S3). We also note that ALS mutations did not accelerate ANS-positive aggregation in the exponential regime (Table S3). For example, the rate of exponential aggregate formation of E100K and D90A apo-SOD1$^{90\%2SH}$ was lower than WT apo-SOD1$^{90\%2SH}$, however, A4V showed statistically similar rates of exponential aggregation as WT apo-SOD1$^{90\%2SH}$ (Table S3).

The results of ANS and ThT fluorescence suggest that wells that exhibit exponential, amorphous aggregation, according to ANS fluorescence, will produce late fibril lag time, slow fibril propagation, and weak fluorescence in ThT assays. Thus, the amorphous and fibrillar aggregation of SOD1 appears to occur in stochastic competition, and whichever process initiates first will

DOI: 10.1021/acschemneuro.6b00048
ACS Chem. Neurosci. 2016, 7, 799−810

propagate first and flourish, while diminishing the amount of SOD1 available for competing pathways of aggregation. The rapid, exponential aggregation of SOD1 into amorphous oligomers is reflective of a stochastic shunt, by which the SOD1 protein can bypass fibrillar pathways of aggregation and rapidly form large amorphous species (Figure 7d).

Aggregation of Apo-SOD1 (Measured by DLS) Is Stochastic and Nonuniformly Accelerated by ALS Mutations. Because ThT fluorescence cannot detect non-amyloid (e.g., amorphous) or protofibrillar oligomers that might not bind ThT (both of which might be toxic species in ALS[2]), we also used DLS to measure the rate of formation of SOD1 aggregates, and to quantify the rate of disappearance of monomeric apo-SOD1. In these experiments, solutions of WT and ALS-variant apo-SOD1$^{90\%2SH}$ that were analyzed with DLS were treated identically to solutions in standard ThT assays (i.e., agitated in microplate wells, with Teflon beads, in the presence of ThT). DLS measurements were carried out on 33 wells for each ALS variant.

All apo-SOD1$^{90\%2SH}$ proteins exhibited, according to DLS, stochastic aggregation kinetics with a large range in individual lag times of >10 h, in agreement with their fibrillization kinetics (Figure S8 contains three representative kinetic plots for each mutant). The approximate lag times of aggregation, interpolated from plots of average radii (R_H) of all species, versus time, were only 2 h (Figure 8a), that is, several hours earlier than the mean lag time of fibrillization in complementary ThT fluorescence assays (Figure 2). This result suggests that ThT-negative SOD1 oligomers form before mature fibrillar assemblies. The plots of R_H versus time for D90A and WT apo-SOD1$^{90\%2SH}$ were superimposable (Figure 8a), suggesting identical rates of aggregation. Extracting exact lag times from plots of R_H versus time was not possible because mathematical fits of iterate plots only yielded $R^2 < 0.6$. To extract statistically meaningful (and comparable) kinetic values of aggregation, we plotted the decay of monomeric apo-SOD1$^{90\%2SH}$, as measured by DLS (Figure 8b).

The decay of monomeric SOD1 was exponential (Figure 8b). The half-life of monomeric WT apo-SOD1$^{90\%2SH}$ was (according to DLS) statistically identical to the half-life of D90A ($p = 0.21$) and E100K ($p = 0.51$), but ~30% faster than A4V apo-SOD1$^{90\%2SH}$ ($p = 0.02$) (Figure 8b). The decay of each monomer coincided with the appearance of at least one intermediate oligomer ($R_H = 10^2$ nm) and an equilibrium oligomer ($R_H = 10^3 - 10^4$ nm) (Figure 8c). In conclusion, ALS mutations do not uniformly accelerate the aggregation of apo-SOD1, as measured by DLS. These results are in contrast to a previous DLS analysis of apo-SOD1 aggregation by Vassal et al.[49] that reported a uniform increase in the rates of aggregation of ALS-variant apo-SOD1, relative to WT apo-SOD1. In this previous study,[49] aggregation rates were calculated from averages of 3−5 replicates for each mutant, which might be insufficient (in our opinion) to accurately express the rate of a process as stochastic as SOD1 aggregation.

Noise and Stochasticity in SOD1 Aggregation. Why is the aggregation of SOD1 into amorphous or fibrillar aggregates stochastic? The most obvious explanation for stochasticity—if there is a singular explanation—is that values of E_a are similar for divergent aggregation pathways that branch from a common, peri-oligomeric state to mature amorphous and/or fibrillar oligomers. Such degeneracies in E_a, despite morphologically different end products (with presumably different equilibrium ΔG), are not far-fetched when considering that the proto-oligomers that precede fibrillization are generally amorphous[50] and might continue propagating amorphous aggregates as easily as fibrillar ones.

What can noise levels associated with ThT and ANS fluorescence tell us about SOD1 aggregation? Noise levels peak during the nucleation phase of fibrillization of all ALS-variant apo-SOD1$^{30\%2SH}$, however, noise decreased for WT apo-SOD1$^{30\%2SH}$ during the nucleation phase (Figure 9a). Noise

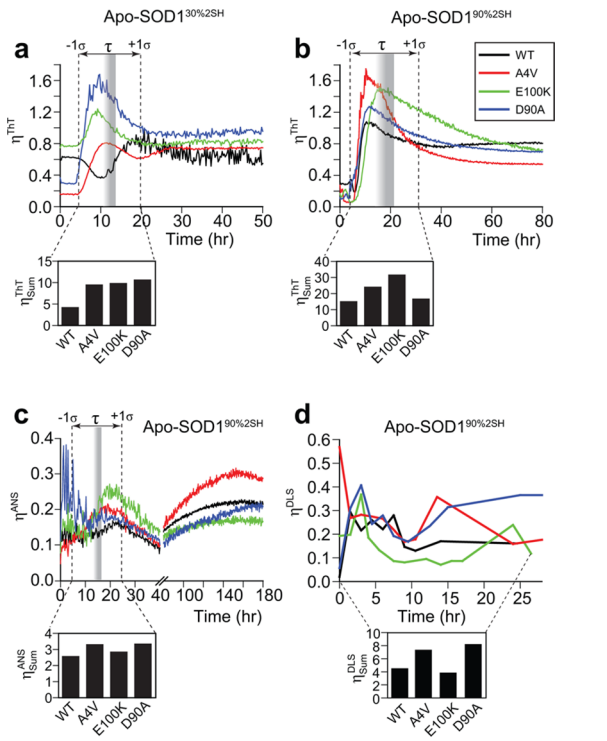

Figure 9. Noise (variability) associated with SOD1 oligomer nucleation is increased by ALS mutations. Kinetic plots of oligomer noise (η) associated with ThT fluorescence amyloid assays (a,b), ANS aggregate assays (c), and DLS nonamyloid aggregation assays (d) of WT and ALS-variant apo-SOD1 from Figures 1, 2, 7, and 8, respectively. The shaded bar in (a−c) represents the range of mean lag time (τ) for all proteins, and dashed lines indicate one standard deviation (σ) from mean lag time. Insets below panels (a−c) show plots of total noise (η_{Sum}) associated with the nucleation of oligomeric apo-SOD1. η_{Sum} was quantified via integration of noise plots over the time domain corresponding to $\tau \pm 1\sigma$. η_{Sum} for inset in panel (d) was calculated via integration of DLS noise plots over the entire experimental time period.

levels also peak during the nucleation of apo-SOD1$^{90\%2SH}$ in ANS and ThT assays (however, the WT protein did not undergo a decrease in noise during nucleation; Figure 9b,c). Moreover, ALS mutations uniformly increase the noise associated with oligomer nucleation (see inset bar graphs in Figure 9), as measured by ThT and ANS fluorescence. The noise associated with aggregation of mutant apo-SOD1$^{90\%2SH}$, as measured by DLS, was not decreased compared to that of the WT protein (Figure 9d). We hypothesize that WT SOD1 nucleation is generally less noisy than ALS-variant SOD1 nucleation because its energy landscape of oligomerization contains fewer kinetically bistable states, that is, fewer pathways of oligomerization with similar E_a.

The fact that the nucleation of oligomers composed of ALS-variant SOD1 is "noisier" than that of WT SOD1 suggests that the nucleation of an individual population of ALS-variant SOD1 proteins will be less predictable and less reflective of mean

DOI: 10.1021/acschemneuro.6b00048
ACS Chem. Neurosci. 2016, 7, 799−810

nucleation rates. An ALS mutation can, for example, increase the rate of aggregation of a single population of SOD1 proteins—that is, the discrete isolated population of SOD1 within a single cell (or here, microplate well)—without increasing the mean rate of aggregation of the entire population of cells or wells. This ability to accelerate aggregation by increasing noise can be seen in Figures 1a and S2: the fastest replicates of ALS-variant apo-SOD1$^{30\%2SH}$ have shorter lag times than the fastest replicates of the WT apo-SOD1$^{30\%2SH}$. Conversely, the slowest wells to aggregate among all ALS-variant apo-SOD1$^{30\%2SH}$ data sets aggregated more slowly than the slowest replicates of WT apo-SOD1$^{30\%2SH}$.

Implications of Oligomer Noise and Stochasticity in Prionlike Aggregation. The results of this study establish three implications for rationalizing in vitro SOD1 aggregation data with clinical phenotypes of ALS: (i) attempting to correlate *in vitro* lag times and propagation rates with in vivo data (e.g., age of disease onset, survival time after onset) will require mean values that are statistically significant (i.e., calculated from $\geq 10^2$ replicates), (ii) the "noise" of nucleation and propagation might be more important in pathogenesis than mean rates of nucleation and propagation, and (iii) the statistical distribution of iterate lag times and propagation rates (i.e., log-normal distributions) might be useful in rationalizing variation in clinical phenotypes associated with a particular mutation. Regarding point (ii), the noise associated with aggregation can play a role in prionlike mechanisms of aggregation. It is reasonable to hypothesize that a mutation can accelerate the aggregation of SOD1 by increasing noise, without increasing mean rates of aggregation. In other words, pathogenesis might be triggered by rapid aggregation in a minor fraction of motor neurons (i.e., noise), wherein oligomeric SOD1 from these cells subsequently infects other cells.

Regarding point (iii), the distribution of onset age for 30 ALS patients with the L144F *SOD1* mutation (the only ALS-*SOD1* mutation we could find with individual ages of onset for a set of $n > 10$ patients) is log−normal ($R^2 = 0.99$, Figure S9). Log−normal distributions describe the underlying probability distribution for many stochastic biological phenomena, for example, the latency period of human diseases and variations in the age of onset of other neurodegenerative diseases linked to protein aggregation.[51]

CONCLUSION

The SOD1 apo protein proceeds down two divergent, kinetically similar pathways of aggregation—amyloid and amorphous aggregation—and these pathways are followed stochastically. Whichever pathway is initiated first will flourish (in vitro) while the other pathway will be diminished via removal of soluble SOD1 by the competing pathway. In other words, some wells will generate oligomers that are more fibrillar and less amorphous, while others will generate less fibrillar and more amorphous oligomers (both types of oligomers are observed in vivo[2,7]). This conclusion not only explains the perplexing variability in ThT amyloid assays of SOD1,[7,22] but suggests that an isolated population of SOD1—for example, in an individual microplate well, or analogously in a single motor neuron—can stochastically diverge toward catastrophic oligomerization before populations of SOD1 in neighboring cells/wells.

ALS-linked mutations can also accelerate or decelerate the aggregation of individual populations of SOD1 (i.e., an individual well or cell) without altering mean rates of aggregation of the entire set of wells (or cells), via increasing the noise associated with oligomer nucleation and propagation. All ALS mutations studied in this paper—including cryptic mutations that have minimal effects on the biophysical properties of SOD1—did not uniformly increase the mean rate of nucleation or propagation of fibrils, but did uniformly increase the noise level associated with fibrillization, that is, increased the probability that SOD1 will *sometimes* self-assemble at rates (and morphologies) that are far from mean values for the WT protein (Figure 8). The stochasticity associated with SOD1 oligomerization (in vitro), and the effects of ALS mutations on oligomer noise provides a quantitative mechanism for rationalizing the prionlike initiation of misfolded SOD1 in one neuronal cell and propagation of the oligomer to other cells in the central nervous system.

In particular, the stochastic nature of SOD1 aggregation provides a plausible molecular mechanism for McInnes' "one-hit" model of neurodegeneration in ALS.[52,53] The "one-hit" model (analogous to Knudson's two-hit hypothesis for oncogenesis[54]) suggests that neurodegeneration initiates as a result of a random, catastrophic event inside one cell, followed by propagation to neighboring cells. The "one hit" model is based upon the exponential increase in probability of neuronal cell death with age, in contrast to the cumulative damage model that predicts linear increments in neuronal cell death. The results of the current study suggest that a fraction of individual populations of SOD1—that is, a fraction of motor neurons—have the intrinsic propensity to undergo rapid, catastrophic self-assembly into neurotoxic oligomers (with rates and morphologies far from the mean) while populations in neighboring cells do not produce a similarly toxic mixture of oligomers, at a similarly rapid rate. The probability that this rare, catastrophic self-assembly might occur in a motor neuron might be increased by pathogenic mutations that increase the noise associated with oligomer nucleation.

METHODS

SOD1 Purification, Demetalation, and Biophysical Characterization. WT and ALS-variant SOD1 proteins were recombinantly expressed in *S. cerevisiae*, purified, and demetalated, as previously described.[22] The absence of metal ions was confirmed with inductively coupled plasma mass spectrometry (ICP-MS). Protein purity, thermostability, and lack of tryptophan oxidation were confirmed with mass spectrometry and differential scanning calorimetry, as previously described.[22]

Apo-SOD1$^{30\%2SH}$ (~30% disulfide reduction) was prepared by incubating apo-SOD1^{S-S} in 10 mM TCEP (pH 7.4, 22 °C) with mild orbital shaking (90 rpm) for 6 h prior to initiation of aggregation assay with Teflon beads and rapid shaking (360 rpm). Apo-SOD1$^{90\%2SH}$ (>90% disulfide reduction) was generated by incubating apo-SOD1^{S-S} in 100 mM TCEP (pH 7.4, 22 °C), with orbital shaking (90 rpm), for 6 h. The degree of disulfide reduction was estimated with differential scanning calorimetry, based upon the T_m values for fully oxidized and fully reduced proteins. The degree of monomerization for WT and ALS-variant apo-SOD1 proteins was determined with size-exclusion chromatography using a Zorbax G250 column coupled to a photodiode array (PDA) detector, as previously described.[22] Differential scanning calorimetry was performed with a Microcal LLC VP-DSC at [SOD1] = 2 mg/mL (10 mM KPO_4, pH 7.4), as previously described.[22] Electrospray ionization mass spectrometry was performed on an LTQ LX/Orbitrap Discovery ESI-MS (Thermo Scientific) instrument, as previously described.[22]

Thioflavin-T (ThT) and 1-Anilino-8-naphthalenesulfonate (ANS) Fluorescence Aggregation Assays. High-throughput ThT and ANS aggregation assays were performed in a 96-well microplate, as previously described.[22] See the Supporting Information for details on replicate assays that were performed on reused Teflon beads and microplates.

DOI: 10.1021/acschemneuro.6b00048
ACS Chem. Neurosci. 2016, 7, 799−810

Dynamic Light Scattering. Dynamic light scattering (DLS) experiments were performed with a DynaPro Nanostar instrument (Wyatt Technology, Santa Barbara, CA). The following parameters were set for all measurements: peak radius low cutoff, 0.5 nm; peak radius high cutoff, 10^4 nm; correlation function low cutoff, 1.5 μs; correlation function high cutoff, 6×10^4 μs. For each DLS assay, a 10 μL aliquot of each well was used and results were reported as the average of 10 consecutive autocorrelation functions (acquisition time = 5 s). Kinetic DLS assays were carried out on aliquots taken from wells of microplates. Protein solutions in microplates were prepared and treated identically as in ThT amyloid assays (i.e., filtered, shaken with rotary agitation using a Fluoroskan plate reader and Teflon beads) and ThT was added.

Transmission Electron Microscopy (TEM). Morphology of resultant aggregates of all apo-SOD1 proteins (fibrillar or amorphous) after ThT/ANS and DLS assays was determined with a JEOL 1230 high contrast transmission electron microscope operating at 80 kV, as described elsewhere.[22]

■ ASSOCIATED CONTENT

Supporting Information

The Supporting Information is available free of charge on the ACS Publications website at DOI: 10.1021/acschemneuro.6b00048.

Further details on ThT and ANS fluorescence aggregation assays, well- and bead-specific aggregation assays, statistical analyses, DSC thermograms and size-exclusion chromatograms, ThT fluorescence scatter plots, correlation of lag time and inverse propagation rate at different rpms, ThT fluorescence scatter plots at different temperatures, noise plots at different shaking speeds, temperatures, and monomer concentrations, ANS fluorescence scatter plots, DLS scatter plots, age of disease onset histogram for L144F SOD1, ICP-MS data, kinetic parameters for ThT and ANS fluorescence assays, and supporting references (PDF)

■ AUTHOR INFORMATION

Corresponding Author

*E-mail: Bryan_Shaw@baylor.edu.

Author Contributions

A.A and B.F.S. organized the research. All the authors contributed to the design of the experiments, the analysis of the data, and editing of the manuscript.

Funding

Financial support for this research was provided to BFS by the Department of Defense (W81XWH-11-1-0790), the National Science Foundation (CHE: 1352122), and the Welch Foundation (AA-1854).

Notes

The authors declare no competing financial interest.

■ ACKNOWLEDGMENTS

The authors would like to thank Dr. Bernd Zechmann (Center for Microscopy and Imaging, Baylor University) for technical support with microscopy and image analysis.

■ REFERENCES

(1) Chattopadhyay, M., Durazo, A., Sohn, S. H., Strong, C. D., Gralla, E. B., Whitelegge, J. P., and Valentine, J. S. (2008) Initiation and elongation in fibrillation of ALS-linked superoxide dismutase. *Proc. Natl. Acad. Sci. U. S. A. 105*, 18663−18668.

(2) Kerman, A., Liu, H. N., Croul, S., Bilbao, J., Rogaeva, E., Zinman, L., Robertson, J., and Chakrabartty, A. (2010) Amyotrophic lateral sclerosis is a non-amyloid disease in which extensive misfolding of SOD1 is unique to the familial form. *Acta Neuropathol. 119*, 335−344.

(3) Rotunno, M. S., and Bosco, D. A. (2013) An emerging role for misfolded wild-type SOD1 in sporadic ALS pathogenesis. *Front. Cell. Neurosci. 7*, 253.

(4) Munch, C., O'Brien, J., and Bertolotti, A. (2011) Prion-like propagation of mutant superoxide dismutase-1 misfolding in neuronal cells. *Proc. Natl. Acad. Sci. U. S. A. 108*, 3548−3553.

(5) Lee, S., and Kim, H. J. (2015) Prion-like Mechanism in Amyotrophic Lateral Sclerosis: are Protein Aggregates the Key? *Exp. Neurobiol. 24*, 1−7.

(6) Ayers, J. I., Fromholt, S. E., O'Neal, V. M., Diamond, J. H., and Borchelt, D. R. (2016) Prion-like propagation of mutant SOD1 misfolding and motor neuron disease spread along neuroanatomical pathways. *Acta Neuropathol. 131*, 103−114.

(7) Lang, L., Zetterstrom, P., Brannstrom, T., Marklund, S. L., Danielsson, J., and Oliveberg, M. (2015) SOD1 aggregation in ALS mice shows simplistic test tube behavior. *Proc. Natl. Acad. Sci. U. S. A. 112*, 9878−9883.

(8) Lang, L., Kurnik, M., Danielsson, J., and Oliveberg, M. (2012) Fibrillation precursor of superoxide dismutase 1 revealed by gradual tuning of the protein-folding equilibrium. *Proc. Natl. Acad. Sci. U. S. A. 109*, 17868−17873.

(9) Xue, W. F., Homans, S. W., and Radford, S. E. (2008) Systematic analysis of nucleation-dependent polymerization reveals new insights into the mechanism of amyloid self-assembly. *Proc. Natl. Acad. Sci. U. S. A. 105*, 8926−8931.

(10) Hortschansky, P., Schroeckh, V., Christopeit, T., Zandomeneghi, G., and Fandrich, M. (2005) The aggregation kinetics of Alzheimer's β-amyloid peptide is controlled by stochastic nucleation. *Protein Sci. 14*, 1753−1759.

(11) Vali, G. (2008) Repeatability and randomness in heterogeneous freezing nucleation. *Atmos. Chem. Phys. 8*, 5017−5031.

(12) Cao, Z., and Ferrone, F. A. (1997) Homogeneous nucleation in sickle hemoglobin: stochastic measurements with a parallel method. *Biophys. J. 72*, 343−352.

(13) Ghag, G., Ghosh, P., Mauro, A., Rangachari, V., and Vaidya, A. (2013) Stability analysis of 4-species A aggregation model: A novel approach to obtaining physically meaningful rate constants. *Appl. Math. Comput. 224*, 205−215.

(14) Hofrichter, J. (1986) Kinetics of sickle hemoglobin polymerization. III. Nucleation rates determined from stochastic fluctuations in polymerization progress curves. *J. Mol. Biol. 189*, 553−571.

(15) Szavits-Nossan, J., Eden, K., Morris, R. J., MacPhee, C. E., Evans, M. R., and Allen, R. J. (2014) Inherent variability in the kinetics of autocatalytic protein self-assembly. *Phys. Rev. Lett. 113*, 098101.

(16) Hellstrand, E., Boland, B., Walsh, D. M., and Linse, S. (2010) Amyloid β-protein aggregation produces highly reproducible kinetic data and occurs by a two-phase process. *ACS Chem. Neurosci. 1*, 13−18.

(17) Querido, E., Gallardo, F., Beaudoin, M., Menard, C., and Chartrand, P. (2011) Stochastic and reversible aggregation of mRNA with expanded CUG-triplet repeats. *J. Cell Sci. 124*, 1703−1714.

(18) Elowitz, M. B., Levine, A. J., Siggia, E. D., and Swain, P. S. (2002) Stochastic gene expression in a single cell. *Science 297*, 1183−1186.

(19) Gregor, T., Fujimoto, K., Masaki, N., and Sawai, S. (2010) The onset of collective behavior in social amoebae. *Science 328*, 1021−1025.

(20) Giehm, L., and Otzen, D. E. (2010) Strategies to increase the reproducibility of protein fibrillization in plate reader assays. *Anal. Biochem. 400*, 270−281.

(21) Shi, Y., Rhodes, N. R., Abdolvahabi, A., Kohn, T., Cook, N. P., Marti, A. A., and Shaw, B. F. (2013) Deamidation of asparagine to aspartate destabilizes Cu, Zn superoxide dismutase, accelerates fibrillization, and mirrors ALS-linked mutations. *J. Am. Chem. Soc. 135*, 15897−15908.

(22) Abdolvahabi, A., Shi, Y., Rhodes, N. R., Cook, N. P., Marti, A. A., and Shaw, B. F. (2015) Arresting amyloid with coulomb's law: acetylation of ALS-linked SOD1 by aspirin impedes aggregation. *Biophys. J. 108*, 1199−1212.

DOI: 10.1021/acschemneuro.6b00048
ACS Chem. Neurosci. 2016, 7, 799−810

(23) Furukawa, Y., Kaneko, K., Yamanaka, K., and Nukina, N. (2010) Mutation-dependent polymorphism of Cu,Zn-superoxide dismutase aggregates in the familial form of amyotrophic lateral sclerosis. *J. Biol. Chem. 285*, 22221−22231.
(24) Vassall, K. A., Stubbs, H. R., Primmer, H. A., Tong, M. S., Sullivan, S. M., Sobering, R., Srinivasan, S., Briere, L. A. K., Dunn, S. D., Colón, W., and Meiering, E. M. (2011) Decreased stability and increased formation of soluble aggregates by immature superoxide dismutase do not account for disease severity in ALS. *Proc. Natl. Acad. Sci. U. S. A. 108*, 2210−2215.
(25) Pratt, A. J., Shin, D. S., Merz, G. E., Rambo, R. P., Lancaster, W. A., Dyer, K. N., Borbat, P. P., Poole, F. L., 2nd, Adams, M. W., Freed, J. H., Crane, B. R., Tainer, J. A., and Getzoff, E. D. (2014) Aggregation propensities of superoxide dismutase G93 hotspot mutants mirror ALS clinical phenotypes. *Proc. Natl. Acad. Sci. U. S. A. 111*, E4568−4576.
(26) Bergh, J., Zetterstrom, P., Andersen, P. M., Brannstrom, T., Graffmo, K. S., Jonsson, P. A., Lang, L., Danielsson, J., Oliveberg, M., and Marklund, S. L. (2015) Structural and kinetic analysis of protein-aggregate strains *in vivo* using binary epitope mapping. *Proc. Natl. Acad. Sci. U. S. A. 112*, 4489−4494.
(27) Crisp, M. J., Mawuenyega, K. G., Patterson, B. W., Reddy, N. C., Chott, R., Self, W. K., Weihl, C. C., Jockel-Balsarotti, J., Varadhachary, A. S., Bucelli, R. C., Yarasheski, K. E., Bateman, R. J., and Miller, T. M. (2015) *In vivo* kinetic approach reveals slow SOD1 turnover in the CNS. *J. Clin. Invest. 125*, 2772−2780.
(28) Wang, J., Slunt, H., Gonzales, V., Fromholt, D., Coonfield, M., Copeland, N. G., Jenkins, N. A., and Borchelt, D. R. (2003) Copper-binding-site-null SOD1 causes ALS in transgenic mice: aggregates of non-native SOD1 delineate a common feature. *Hum. Mol. Genet. 12*, 2753−2764.
(29) Wang, J., Xu, G., and Borchelt, D. R. (2002) High molecular weight complexes of mutant superoxide dismutase 1: age-dependent and tissue-specific accumulation. *Neurobiol. Dis. 9*, 139−148.
(30) Shaw, B. F., Moustakas, D. T., Whitelegge, J. P., and Faull, K. F. (2010) Taking charge of proteins from neurodegeneration to industrial biotechnology. *Adv. Protein Chem. Struct. Biol. 79*, 127−164.
(31) Knowles, T. P., Waudby, C. A., Devlin, G. L., Cohen, S. I., Aguzzi, A., Vendruscolo, M., Terentjev, E. M., Welland, M. E., and Dobson, C. M. (2009) An analytical solution to the kinetics of breakable filament assembly. *Science 326*, 1533−1537.
(32) Tiwari, A., and Hayward, L. J. (2003) Familial amyotrophic lateral sclerosis mutants of copper/zinc superoxide dismutase are susceptible to disulfide reduction. *J. Biol. Chem. 278*, 5984−5992.
(33) Doucette, P. A., Whitson, L. J., Cao, X., Schirf, V., Demeler, B., Valentine, J. S., Hansen, J. C., and Hart, P. J. (2004) Dissociation of human copper-zinc superoxide dismutase dimers using chaotrope and reductant. Insights into the molecular basis for dimer stability. *J. Biol. Chem. 279*, 54558−54566.
(34) Rodriguez, J. A., Shaw, B. F., Durazo, A., Sohn, S. H., Doucette, P. A., Nersissian, A. M., Faull, K. F., Eggers, D. K., Tiwari, A., Hayward, L. J., and Valentine, J. S. (2005) Destabilization of apoprotein is insufficient to explain Cu,Zn-superoxide dismutase-linked ALS pathogenesis. *Proc. Natl. Acad. Sci. U. S. A. 102*, 10516−10521.
(35) Leal, S. S., Cristovao, J. S., Biesemeier, A., Cardoso, I., and Gomes, C. M. (2015) Aberrant zinc binding to immature conformers of metal-free copper-zinc superoxide dismutase triggers amorphous aggregation. *Metallomics 7*, 333−346.
(36) Fodera, V., Librizzi, F., Groenning, M., van de Weert, M., and Leone, M. (2008) Secondary nucleation and accessible surface in insulin amyloid fibril formation. *J. Phys. Chem. B 112*, 3853−3858.
(37) Morris, R. J., Eden, K., Yarwood, R., Jourdain, L., Allen, R. J., and Macphee, C. E. (2013) Mechanistic and environmental control of the prevalence and lifetime of amyloid oligomers. *Nat. Commun. 4*, 1891−1899.
(38) Ferreira, A. S., da Silva, M. A., and Cressoni, J. C. (2003) Stochastic modeling approach to the incubation time of prionic diseases. *Phys. Rev. Lett. 90*, 198101−198105.
(39) Colby, D. W., Cassady, J. P., Lin, G. C., Ingram, V. M., and Wittrup, K. D. (2006) Stochastic kinetics of intracellular huntingtin aggregate formation. *Nat. Chem. Biol. 2*, 319−323.
(40) Oxtoby, D. W. (1998) Nucleation of first-order phase transitions. *Acc. Chem. Res. 31*, 91−97.
(41) Yoshimura, Y., Lin, Y., Yagi, H., Lee, Y. H., Kitayama, H., Sakurai, K., So, M., Ogi, H., Naiki, H., and Goto, Y. (2012) Distinguishing crystal-like amyloid fibrils and glass-like amorphous aggregates from their kinetics of formation. *Proc. Natl. Acad. Sci. U. S. A. 109*, 14446−14451.
(42) Shaw, B. F., and Valentine, J. S. (2007) How do ALS-associated mutations in superoxide dismutase 1 promote aggregation of the protein? *Trends Biochem. Sci. 32*, 78−85.
(43) Zhu, M., Souillac, P. O., Ionescu-Zanetti, C., Carter, S. A., and Fink, A. L. (2002) Surface-catalyzed amyloid fibril formation. *J. Biol. Chem. 277*, 50914−50922.
(44) Vacha, R., Linse, S., and Lund, M. (2014) Surface effects on aggregation kinetics of amyloidogenic peptides. *J. Am. Chem. Soc. 136*, 11776−11782.
(45) Fandrich, M. (2007) Absolute correlation between lag time and growth rate in the spontaneous formation of several amyloid-like aggregates and fibrils. *J. Mol. Biol. 365*, 1266−1270.
(46) Wright, G. S., Antonyuk, S. V., Kershaw, N. M., Strange, R. W., and Samar Hasnain, S. (2013) Ligand binding and aggregation of pathogenic SOD1. *Nat. Commun. 4*, 1758.
(47) Younan, N. D., and Viles, J. H. (2015) A Comparison of Three Fluorophores for the Detection of Amyloid Fibers and Prefibrillar Oligomeric Assemblies. ThT (Thioflavin T); ANS (1-Anilinonaphthalene-8-sulfonic Acid); and bisANS (4,4′-Dianilino-1,1′-binaphthyl-5,5′-disulfonic Acid). *Biochemistry 54*, 4297−4306.
(48) Hawe, A., Sutter, M., and Jiskoot, W. (2008) Extrinsic fluorescent dyes as tools for protein characterization. *Pharm. Res. 25*, 1487−1499.
(49) Vassall, K. A., Stubbs, H. R., Primmer, H. A., Tong, M. S., Sullivan, S. M., Sobering, R., Srinivasan, S., Briere, L. A., Dunn, S. D., Colon, W., and Meiering, E. M. (2011) Decreased stability and increased formation of soluble aggregates by immature superoxide dismutase do not account for disease severity in ALS. *Proc. Natl. Acad. Sci. U. S. A. 108*, 2210−2215.
(50) Ghosh, D., Singh, P. K., Sahay, S., Jha, N. N., Jacob, R. S., Sen, S., Kumar, A., Riek, R., and Maji, S. K. (2015) Structure based aggregation studies reveal the presence of helix-rich intermediate during alpha-Synuclein aggregation. *Sci. Rep. 5*, 9228−9243.
(51) Limpert, E., Stahel, W. A., and Abbt, M. (2001) Log-normal Distributions across the Sciences: Keys and Clues: On the charms of statistics, and how mechanical models resembling gambling machines offer a link to a handy way to characterize log-normal distributions, which can provide deeper insight into variability and probability—normal or log-normal: That is the question. *BioScience 51*, 341−352.
(52) Clarke, G., Collins, R. A., Leavitt, B. R., Andrews, D. F., Hayden, M. R., Lumsden, C. J., and McInnes, R. R. (2000) A one-hit model of cell death in inherited neuronal degenerations. *Nature 406*, 195−199.
(53) Clarke, G., and Lumsden, C. J. (2005) Heterogeneous cellular environments modulate one-hit neuronal death kinetics. *Brain Res. Bull. 65*, 59−67.
(54) Knudson, A. G., Jr. (1971) Mutation and cancer: statistical study of retinoblastoma. *Proc. Natl. Acad. Sci. U. S. A. 68*, 820−823.

DOI: 10.1021/acschemneuro.6b00048
ACS Chem. Neurosci. 2016, 7, 799−810